HiSST: 3rd International Conference on
High-Speed Vehicle Science Technology
14 -19 April 2024, Busan, Korea

An Experimental Investigation on Pressure Drop Characteristics of Microchannel Heat Sink to Ensure Flow Stability of Boiling Heat Transfer

*Taeho Choi, Tae Young Kim**
Department of Mechanical and Automotive Engineering, Seoul National University of Science and Technology, 232 Gongneung-ro, Nowon-gu, Seoul 01811, Republic of Korea

Abstract

In the space industry, the management of high heat flux is paramount to ensuring the stability and efficiency of equipment operating in the extreme conditions of space. The ability to effectively dissipate heat generated by onboard electronics is crucial for maintaining operational reliability and preventing overheating, which can lead to performance degradation, reduced lifespan, and mission failure. Within this context, the application of multi-phase heat transfer methodologies has emerged as a promising candidate. Specifically, flow boiling within microchannel heat sinks is regarded as a forefront solution to this challenge, attributed to its superior heat transfer performances. Nevertheless, the rapid vapor expansion within such channels frequently incites flow instabilities, manifesting as significant pressure drop oscillations, which pose a substantial barrier to the reliable application of this technology. This research introduces a pioneering solution to address the aforementioned instability through the development of a Half-range T-shaped channel (HRTC). This innovative design incorporates T-shaped flow paths in the upstream portion and V-shaped grooves in the downstream portion, aiming to attenuate the multiphase flow instabilities inherent to conventional systems. The empirical evidence presented within this study illustrates that the HRTC configuration achieves a substantial diminution in pressure oscillation amplitude, surpassing the performance of traditional T-shaped and plate-fin microchannels by more than fivefold under specified conditions of the heat flux of 63 kW/m^2 and the mass flux of 200 kg/m^{2}s.

Keywords: *Flow boiling*, *Flow instability*, *Flow oscillation*, *Flow reversal*, *Reverse flow*

Nomenclature

Latin
A – area
FFT – Fast Fourier Transform
G – mass flux
HRTC – Half-range T-shaped channel
$\dot{m}$ – mass flow rate
q – heat transfer rate
Greek
β – channel aspect ratio
ρ – density

Subscripts
app – applied
base – base plate
t – total
in – inlet
eff – effective
l – liquid
h – hydraulic
f – fluid
lm – log mean

1. Introduction

1.1. Background [1]

In space operations, effectively managing high heat flux is crucial for the stability and efficiency of equipment subjected to the harsh conditions of space. Efficient heat dissipation from onboard electronics is vital to ensure operational reliability and prevent overheating, which could result in

* *Corresponding author, tykim@seoultech.ac.kr*

degraded performance, shorter equipment lifespan, and potentially compromise mission success. Flow boiling technology is increasingly harnessed in advanced cooling technologies, offering numerous advantages such as high convective heat transfer coefficients, temperature uniformity, relatively low flow rate, and lightweight [1–5]. The use of flow boiling heat transfer in microchannels is one of the attractive cooling techniques that can provide a high heat transfer area per unit volume, making it suitable for high heat flux heat sources. However, under high heat flux conditions, vapor growth within microchannels in the direction from the inlet to the outlet can cause flow instability issues, such as blocking the inflow of liquid or causing backflow in the inlet region [6]. Flow instability hinders the contact of liquid with the microchannel surface, which hampers vapor generation and increases vapor residence time [7,8]. Consequently, this can lead to a reduction in heat transfer performance and issues related to reaching critical heat flux rapidly.

One of the methods to ensure flow stability is to adopt a channel expansion structure in the longitudinal direction, creating a design that facilitates the movement of vapor downstream compared to upstream[9]. Markal et al. [10] proposed the expansion channel, where the number of pin-fins decreases downstream in the expansion channel. The expanded pin-fin design showed a 365% improvement in heat transfer coefficient compared to the pin-fin design without an expansion channel. Furthermore, the system pressure drop for the pin-fin design was 45.2% higher than that of the expanded pin-fin channel. Mathew et al. [11] explored the effects of three channel designs—plain, plate-fin, and a hybrid variant (plate-fin upstream, plain downstream)—on pressure drop, flow instability, and heat transfer. The hybrid channel delayed dry-out at higher heat fluxes due to its better re-wetting ability, attributed to its expanding channel design. Wang et al. [12] investigated the effect of an expanding plate-fin microchannel, measuring 30 mm in length, 0.5 mm in width, and 3.0 mm in height, on flow boiling heat transfer efficiency. The channel, which gradually widens at the outlet to 1.0 mm in width while maintaining a height of 3.0 mm, demonstrated the capability to dissipate heat at a flux rate of up to 270 kW/m^2, more than double that of a straight channel.

In channels where vapor growth is constrained by finned structure, bidirectional growth towards the inlet and outlet occurs. Consequently, increased pressure by vapor growth towards the inlet can hinder liquid inflow, leading to vapor backflow when vapor pressure surpasses liquid inertia. These inter-channel interactions contribute to parallel channel instability (PCI). To alleviate vapor growth constraints and mitigate flow instability, studies have explored methods such as interconnecting channels. By interconnecting channels, flow instability is reduced because it can be expanded to adjacent channels. Raj et al. [13] conducted a comparative investigation into the performance of three distinct microchannel designs: plate-fin microchannel, stepped microchannel (SMC) featuring a V-shaped channel, and stepped diverging microchannel (SDMC) with progressive widening towards the outlet. At a mass flux of 524.45 kg/m^2s and a heat flux of 124 W/cm^2, SDMC exhibited a notable 16 ℃ reduction in wall superheat compared to the plate-fin configuration.

1.2. Objective

Previous studies have primarily focused on designing structures that facilitate effective boiling and increase the critical heat flux. However, while many researchers have examined differential pressures associated with various structures, investigations into flow instability arising alongside bubble growth have been less frequent. Flow instability can lead to phenomena such as clogging due to bubble expansion within the channel, compressibility due to pressure, differences in bubble growth leading to parallel channel instability, and most critically, flow reversal issues. These phenomena can not only alter flow patterns but also simultaneously degrade thermal and differential pressure performance. Therefore, this study proposes the Half-range T-shaped channel (HRTC), aimed at reducing instability caused by vapor growth within microchannels. The HRTC is divided into a microchannel area at the front and a groove area at the rear, based on the center of the channel. Due to the channel's expansion at its center, the HRTC can mitigate vapor, thereby reducing flow instability. Moreover, because the thermal resistance of the microchannel segment is relatively lower compared to the Groove channel, it fosters an environment where bubbles can grow more rapidly and abundantly. Hence, the HRTC concept is designed to not only allow ample bubble growth within the microchannel but also to prevent the discharge and backflow of grown bubbles, effectively suppressing instability.

2. Experimental setup

2.1. Test setup

The experimental setup consists of a micro gear pump, Coriolis mass flow meter, reservoir, preheater, and test section as shown in Fig. 1. A micro gear pump, capable of generating a maximum differential pressure of ~8 bar, was employed. The rpm of the gear pump was adjusted to facilitate circulation of the working fluid, HFE-7100, within the experimental loop. To precisely measure the circulating flow rate, a Coriolis mass flow meter was placed at the rear of the pump. To ensure consistent temperature control of the working fluid entering the test section, a preheater was utilized. The preheater exchanges heat indirectly with a water tank set to a constant temperature, achieving an accuracy of ±0.5°C at the target temperature. Subsequently, the liquid or liquid/vapor mixture exiting the test section enters the degassing chamber. Vapor reaching the degassing chamber is condensed by the reflux condenser situated at its apex, transitioning back into liquid form before circulating within the flow loop.

The test section consists of a polycarbonate plate, PEEK housing, heating block, ceramic insulator, and PEEK insulator, as shown in Fig. 2. The applied heat flux to the test section was adjusted by inserting a total of 12 cartridge heaters into the oxygen-free copper heating block. A 5kW DC power supply was used to vary the input power to achieve the desired heat flux. To investigate flow oscillations, the pressure difference between the inlet and outlet, along with the inlet gauge pressure, was recorded at a sampling rate of 50 ms. Additionally, a high-speed camera capable of capturing images at a frame rate of 1000 fps was employed to observe the interaction between vapor and liquid. Additionally, temperatures at the inlet and outlet, along with the heating block's temperature, were measured using K-type thermocouples. The thermostatic bath was used for maintaining the inlet temperature of the test section during the experiments.

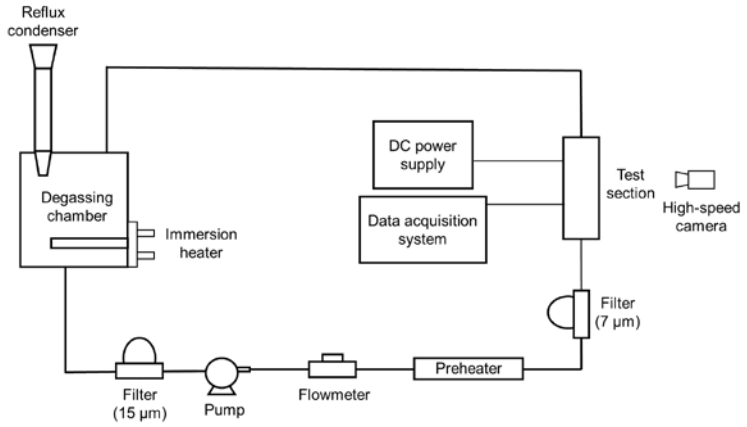

Fig 1. Flow loop of flow boiling experimental setup

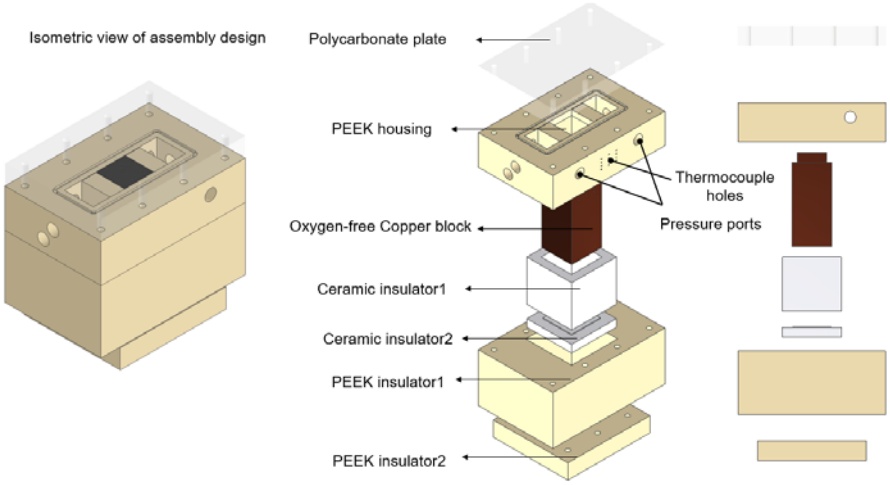

Fig. 2. Schematic diagram of the test section

2.2. Microchannel heat sinks

The test specimens are made of oxygen-free copper, and microchannels were fabricated using the micro-milling method. The proposed microchannel shapes used in this study consist of T-shaped channels in the upstream region and V-shaped grooves in the downstream region. The specimens are composed of four types: Plain, Plate-fin, T-shaped channel, and Half-range T-shaped channel (HRTC) as shown in Fig. 3. The plain surface microchannel possesses a base with dimensions of 20 mm in width and 40 mm in length. The channel, formed by the polycarbonate cover and plain surface, exhibits a hydraulic diameter of 784 μm. In the plate-fin configuration, 25 fins, each measuring 400 μm in width and height, are spaced at equal intervals. The fins covered with a polycarbonate plate form a channel with a hydraulic diameter of 400 μm. In the plate-fin microchannel heat sink design, the section of the fin nearest to the base plate—comprising half of the fin's total height—is thickened by 100 μm along the channel direction, thereby creating a T-shaped microchannel configuration with a hydraulic diameter of 300 μm. The HRTC is equipped with 25 T-shaped channels, each having a hydraulic diameter of 300 μm, oriented in the upstream direction. Additionally, there are 50 V-shaped grooves with a width of 200 μm and an angle of 60° relative to the center of the specimen, positioned in the downstream direction.

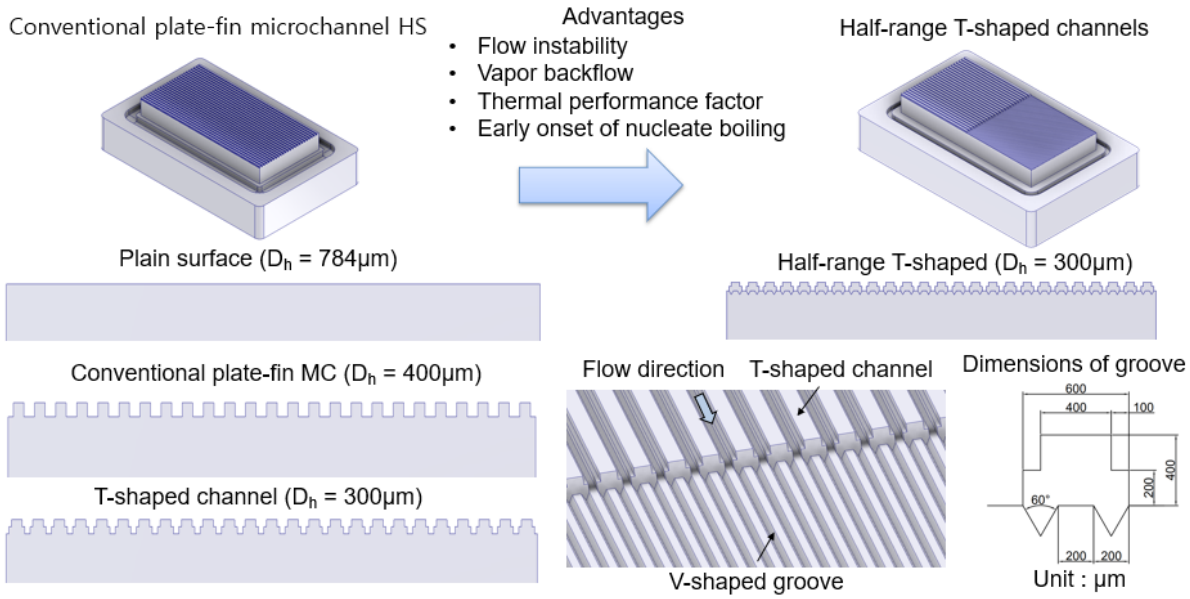

Fig. 3. Four types of microchannels used in this study

2.3. Data reduction

The mass flux of liquid entering the microchannel inlet is expressed as

$$G = \frac{\dot{m}}{A_{in}} \tag{1}$$

where $\dot{m}$ and A_{in} are the mass flow rate and the cross-sectional area of each microchannel at the inlet, respectively. The effective heat flux is expressed as

$$q''_{eff} = \frac{q_{app} - q_{loss}}{A_{base}} \tag{2}$$

Where q_{app}, q_{loss}, and A_{base} are the applied heat transfer rate, heat loss to the environment, and area of the base plate of a microchannel heat sink, respectively. The heat loss is derived in the same way as described in reference [14].

2.4. Validation

To validate the results obtained from the test section, experiments were conducted under laminar flow conditions with single-phase heat transfer. The heat transfer coefficient of single-phase flow is expressed as

$$h = \frac{q_{app} - q_{loss}}{A_t T_{lm}} \tag{3}$$

where A_t and T_{lm} are the total heat transfer area and log-mean temperature difference, respectively. The Nusselt number is expressed as

$$Nu = \frac{hD_h}{k_f} \tag{4}$$

where D_h and k_f are the hydraulic diameter and thermal conductivity of the fluid, respectively.

From the point of view of friction, the friction factor is expressed as

$$f = \Delta P \frac{2D_h}{L} \frac{\rho_l}{G^2} \tag{5}$$

where ΔP, ρ_l, and L are the pressure drop across the heat sink, the density of the liquid phase, and the length of the microchannel heat sink, respectively. To compare the results with this experiment, the Nusselt number was used by the formula proposed by Peng and Peterson [15], and the friction factor was used by the formula proposed by Shah and London [16], and are expressed as follows:

$$Nu = 0.1165 \left(\frac{D_h}{p}\right)^{0.81} \left(\frac{H}{w}\right)^{-0.79} Re^{0.62} Pr^{1/3} \tag{6}$$

$$f = \frac{24}{Re}(1 - 1.3553\beta + 1.9467\beta^2 - 1.7012\beta^3 + 0.9564\beta^4 - 0.2537\beta^5) \tag{7}$$

where the H, p, w, Re, Pr, and β are the height, pitch, and width of fin, Reynolds number, Prandtl number, and aspect ratio of the channel, respectively. Both the Nusselt number and friction factor had errors within a maximum of 12%, confirming that the experimental device was well-designed.

3. Results and Discussion

3.1. Flow pattern

The onset of nucleate boiling in a T-shaped channel occurs at the heat flux of 27 kW/m2 and the mass flux of 200 kg/m^{2}s as shown in Fig. 4(a). As the vapor bubbles move downstream, heat is applied and they expand. The expanded vapor bubbles merge with each other to form elongated bubbles as shown in Fig. 4(b). As depicted in Fig. 4(b), the expansion of the vapor slug towards both the inlet and outlet results in a change in the liquid flow rate entering the channel, attributed to the pressure exerted by the expanding vapor. As a result, the fluctuations of pressure drop across the microchannel heat sink occur according to the heat flux conditions. For a heat flux of 85 kW/m^2, as depicted in Fig. 4(c), the interaction between liquid and vapor intensifies with rapid vapor growth. This leads to the formation of a vapor core in the center of the channel, accompanied by an annular flow where a liquid film develops along the fin. Within this annular flow region, the vapor's expansion force is strong enough to cause backflow in the channel and result in significant pressure fluctuations.

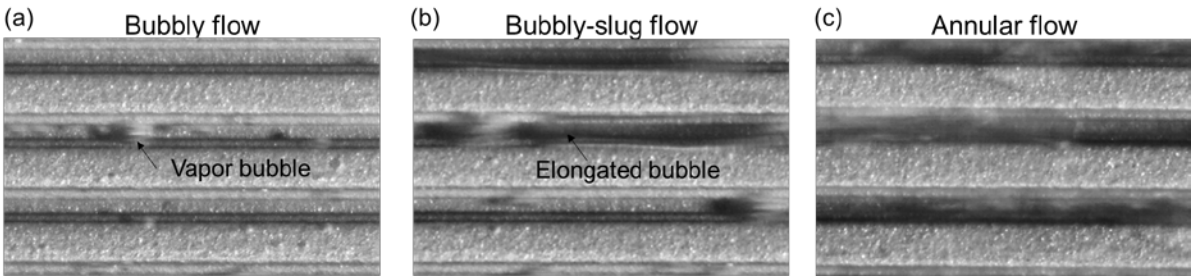

Fig. 4. Flow images of (a) bubbly, (b) bubbly-slug, and (c) annular flow in T-shaped channel at 27, 46, and 85 kW/m^2, respectively, under the mass flux of 200 kg/m^{2}s

3.2. Vapor backflow

Vapor backflow ensues when the pressure exerted by rapidly expanding vapor within the channel surpasses the pressure exerted by the liquid at the inlet. This leads to flow maldistribution, causing more liquid to flow into the remaining channels. Consequently, both system differential pressure and pressure fluctuations escalate due to vapor expansion, resulting in increased pressure volatility. Moreover, as heat flux rises, vapor growth accelerates, leading to more pronounced vapor backflow and heightened pressure oscillation. As depicted in Fig. 5, under a high heat flux condition of 120 kW/m2, vapor rapidly expands within the channel, leading to backflow that fills the inlet with vapor. During this phase, vapor growth obstructs liquid entry into the inlet, reducing expansion power. Liquid replenishment occurs when the pressure from the inlet liquid exceeds that of vapor expansion. Subsequently, vapor compressed by the growing vapor pressure and liquid pressurized by the inlet pump are discharged toward the outlet, creating a chaotic flow pattern as shown in Figure 4(c). This cycle repeats as rapid vaporization occurs on the rewetting surface, perpetuating the backflow phenomenon.

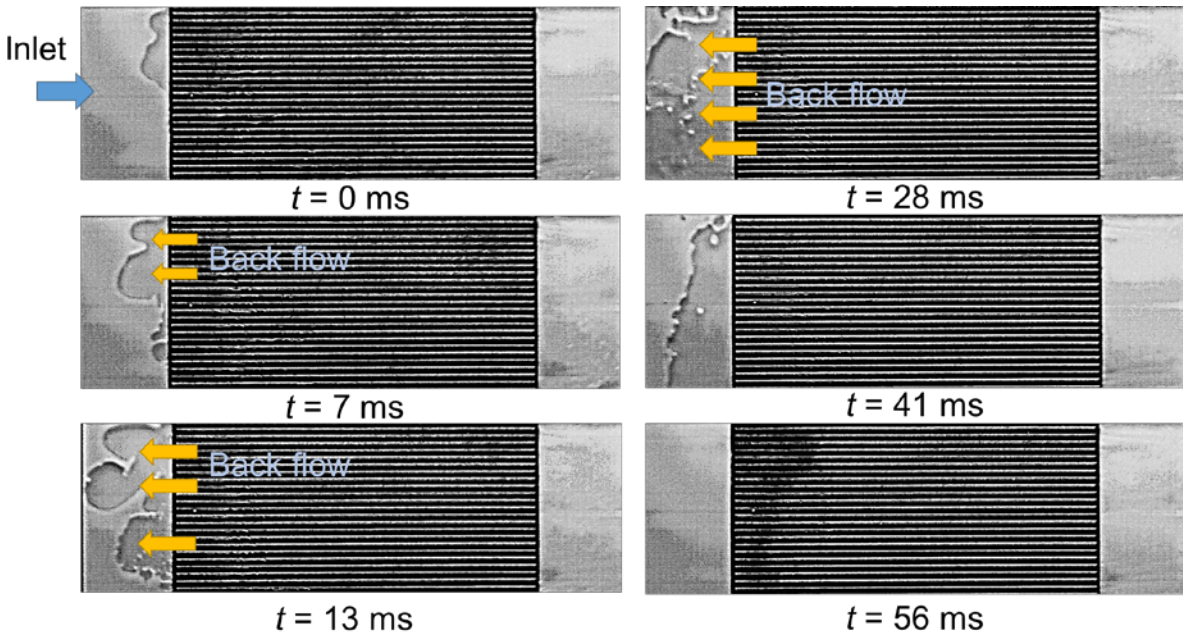

Fig. 5. Vapor backflow phenomena in a T-shaped channel with respect to time at a heat flux of 120 kW/m^2 and the mass flux of 200 kg/m^{2}s

3.3. Flow oscillation

Figure 6 shows pressure oscillation according to heat flux change under the mass flow rate condition of 200 kg/m^{2}s for plain surface, plate-fin, T-shaped channel, and HRTC. In the case of a T-shaped channel, the mass flow rate is less due to the hydraulic diameter, which is 75% of that of the plate-fin, so the outlet vapor quality is higher under the same heat flux and mass flow rate conditions. As the heat flux increases, the frictional pressure drop and accelerational pressure drop increase in the two-phase flow, increasing the average pressure drop. In Fig. 6(a), the appearance of bubbly or slug flow is observed. Pressure oscillations occur randomly due to the expansion of bubbles and slugs growing in multiple channels. The fluctuations in pressure are relatively small, attributable to the confinement of vapor. The results of the Fast Fourier Transform (FFT) analysis for quantitative assessment are presented in Fig. 7, indicating low amplitude across a broad frequency range. As illustrated in Fig. 6(b), in agreement with observations at a lower heat flux of 27 kW/m^2, the T-shaped channel exhibits the highest-pressure oscillations. Conversely, at a heat flux of 63 kW/m^2, the HRTC system demonstrates pressure oscillations nearly akin to those observed in a plain surface configuration, thereby significantly showcasing its effectiveness in mitigating flow instability. The pressure oscillation observed in Fig. 6(c)

for HRTC represents a highly distinctive experimental finding. This is attributed to the presence of a microchannel heatsink in the upstream section of the HRTC configuration, resulting in relatively lower thermal resistance compared to the downstream section. Consequently, even under similar heat flux conditions as other specimens, the heat flux can be concentrated in the upstream section of the HRTC configuration. As a result, under heat flux conditions where the outlet vapor quality approaches 1, flow oscillations surpass those observed in a T-shaped channel at the mass flux of 200 kg/m^{2}s. As depicted in the FFT results presented in Fig. 8, this discrepancy causes the amplitude of HRTC to be approximately twice as high as that of the T-shaped channel. The rapid growth of vapor, which induces flow oscillation and vapor backflow, hampers the delivery of liquid to the fin surfaces, thereby impeding the requisite cooling performance and culminating in Critical Heat Flux (CHF). At a heat flux condition of 120 kW/m^2, the flow oscillation characteristics are observed to be lower than those at a heat flux of 100 kW/m^2 in HRTC as shown in Fig 6(d). This occurs because the rapid growth of vapor leads to the formation of a vapor film on the surface of the fins, disrupting the wetting process of the liquid. As a result, the liquid through the center of the channel, while an inverted-annular flow forms within channels.

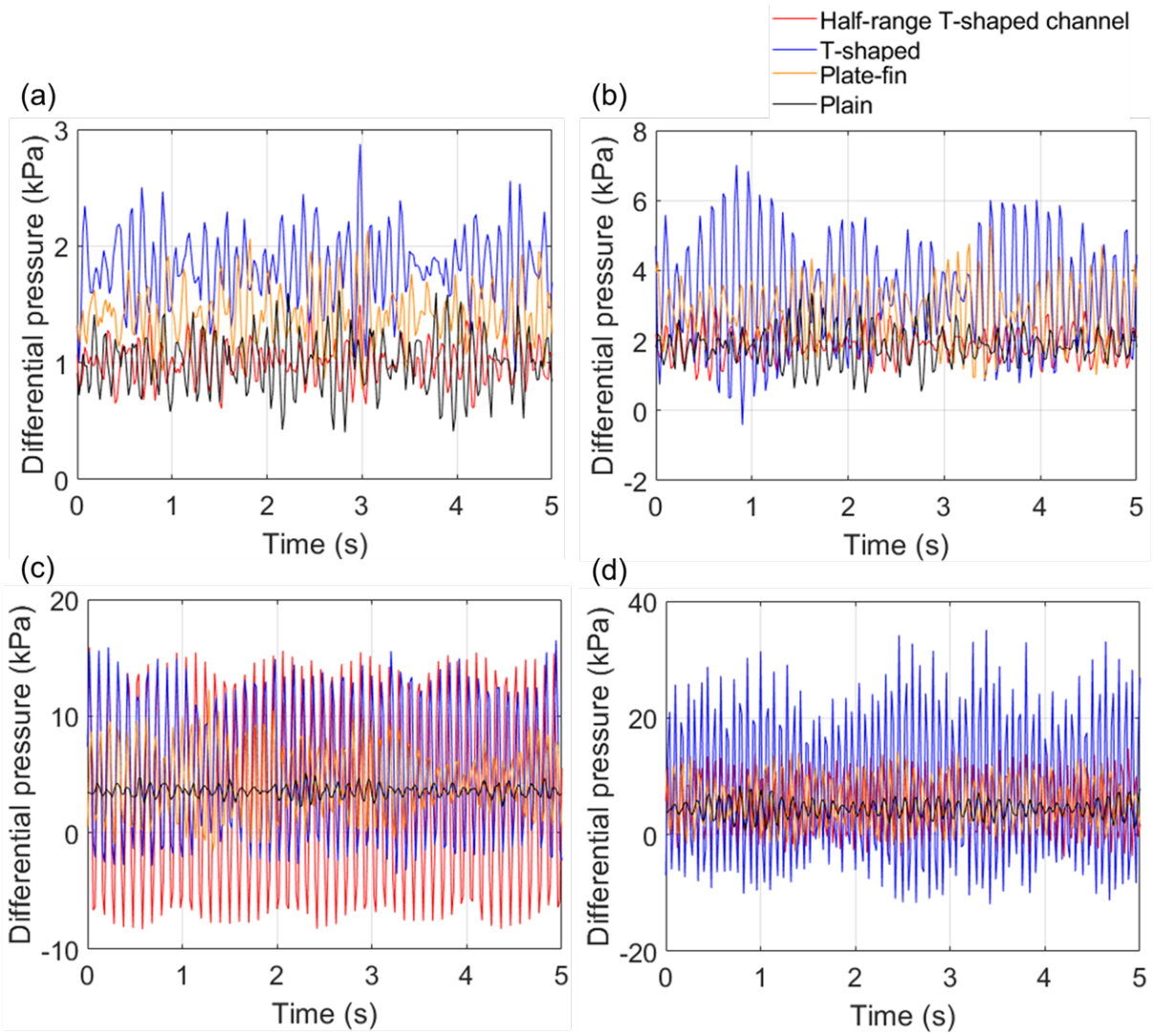

Fig. 6. Pressure oscillations of four-types microchannel heat sinks according to the heat flux of (a) 27 kW/m^2, (b) 63 kW/m^2, (c) 100 kW/m^2, and (d) 120 kW/m^2, respectively, under the mass flux of 200 kg/m^{2}s

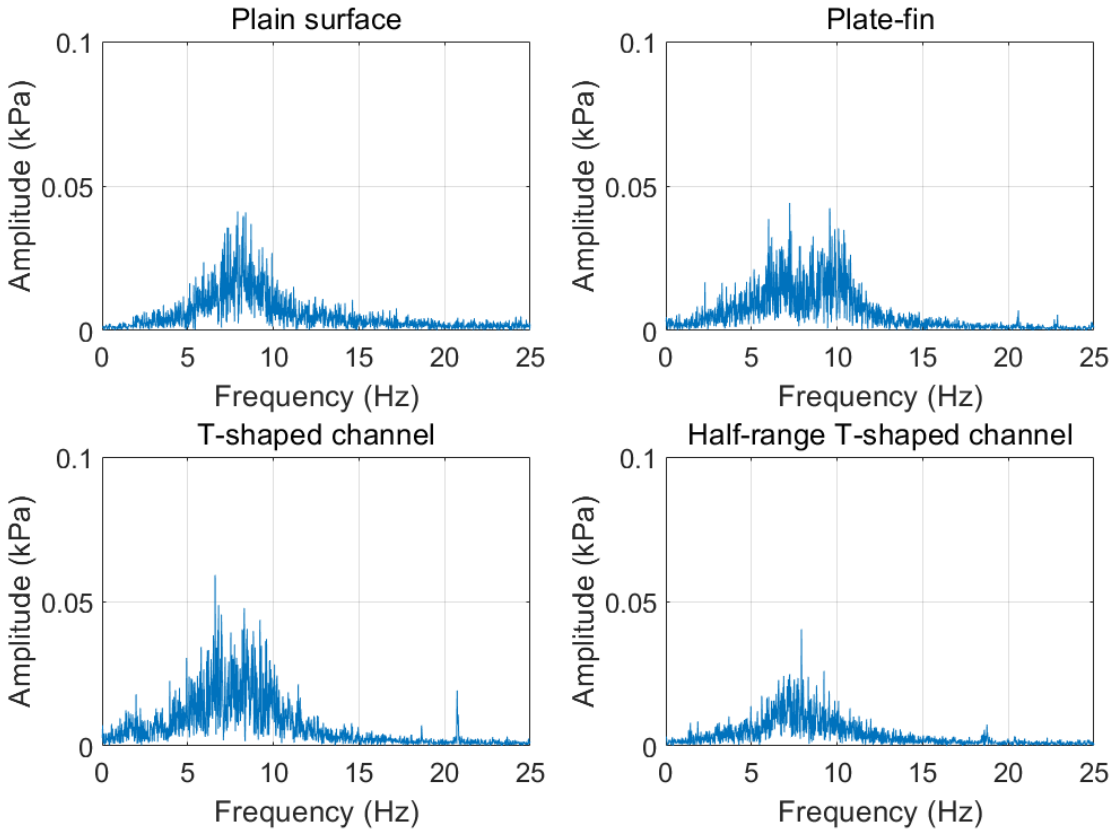

Fig. 7. The results in the frequency domain of pressure drop for four-types microchannel heat sinks at the heat flux of 27 kW/m^2 and the mass flux of 200 kg/m^{2}s

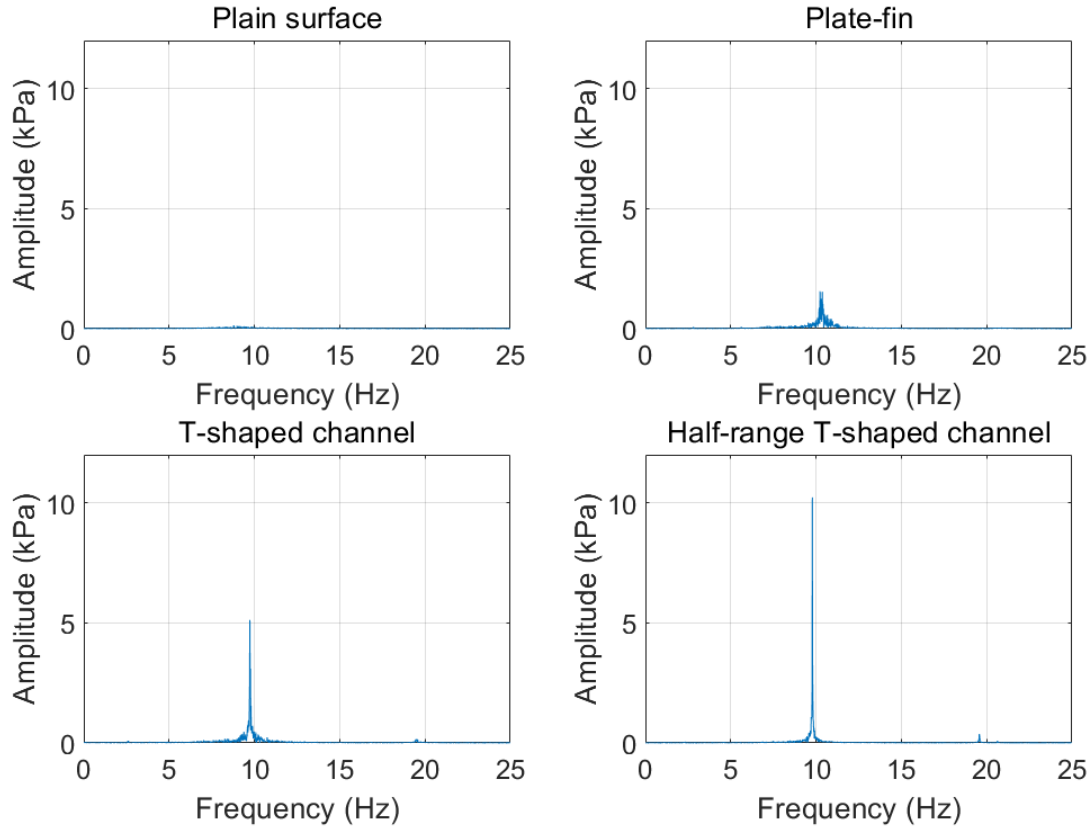

Fig. 8. The results in the frequency domain of pressure drop for four-types microchannel heat sinks at the heat flux of 100 kW/m^2 and the mass flux of 200 kg/m^{2}s

4. Conclusions

In this study, we proposed the half-range T-shaped channel (HRTC) to mitigate flow instability. It was observed that the HRTC reduced flow oscillations compared to the T-shaped channel and plate-fin specimens under the most heat flux conditions at the mass flux of 200 kg/m^{2}s. FFT was used to quantify flow oscillation characteristics, the amplitude of HRTC is lower than the T-shaped channel and plate-fin except for the heat flux condition of 100 kW/m^2. It was determined that the HRTC reaches CHF at an outlet vapor quality of approximately 1, displaying significantly greater oscillation characteristics than both the T-shaped channel and plate-fin. FFT analysis revealed that, under a heat flux condition of 120 kW/m^2, the amplitude of oscillations in the HRTC was about twice that observed in the T-shaped channel.

Acknowledgments

This work was supported by the “A nature-inspired high-efficiency solar energy collector mimicking energy metabolic mechanism of plants” funded by the National Research Foundation (NRF, 2022R1C1C1005922), Republic of Korea, and this work was also supported by Korea Research Institute for defense Technology planning and advancement(KRIT) grant funded by the Korea government (DAPA(Defense Acquisition Program Administration)) (No.KRIT-CT-22-030, Reusable Unmanned Space Vehicle Research Center, 2024).

References

1. V.S. Devahdhanush, Y. Lei, Z. Chen, I. Mudawar, Assessing advantages and disadvantages of macro- and micro-channel flow boiling for high-heat-flux thermal management using computational and theoretical/empirical methods, International Journal of Heat and Mass Transfer 169 (2021) 120787. https://doi.org/10.1016/j.ijheatmasstransfer.2020.120787.
2. S. Halon, Z. Krolicki, R. Revellin, B. Zajaczkowski, Heat transfer characteristics of flow boiling in a micro channel array with various inlet geometries, International Journal of Heat and Mass Transfer 187 (2022) 122549. https://doi.org/10.1016/j.ijheatmasstransfer.2022.122549.
3. J. Zeng, S. Zhang, Y. Tang, Y. Sun, W. Yuan, Flow boiling characteristics of micro-grooved channels with reentrant cavity array at different operational conditions, International Journal of Heat and Mass Transfer 114 (2017) 1001–1012. https://doi.org/10.1016/j.ijheatmasstransfer.2017.06.128.
4. L. Yin, M. Sun, P. Jiang, C. Dang, L. Jia, Heat transfer coefficient and pressure drop of water flow boiling in porous open microchannels heat sink, Applied Thermal Engineering 218 (2023) 119361. https://doi.org/10.1016/j.applthermaleng.2022.119361.
5. W. Gao, X. Xu, X. Liang, Flow boiling of R134a in an open-cell metal foam mini-channel evaporator, International Journal of Heat and Mass Transfer 126 (2018) 103–115. https://doi.org/10.1016/j.ijheatmasstransfer.2018.04.125.
6. H.-G. Kim, Y. Shah, S.-M. Kim, Experimental investigation and analysis of two-phase flow instability of flow boiling in a mini-channel heat sink, International Journal of Heat and Mass Transfer 213 (2023) 124309. https://doi.org/10.1016/j.ijheatmasstransfer.2023.124309.
7. L.E. O’Neill, I. Mudawar, Review of two-phase flow instabilities in macro- and micro-channel systems, International Journal of Heat and Mass Transfer 157 (2020) 119738. https://doi.org/10.1016/j.ijheatmasstransfer.2020.119738.
8. S.M. Sohel Murshed, C.A. Nieto De Castro, A critical review of traditional and emerging techniques and fluids for electronics cooling, Renewable and Sustainable Energy Reviews 78 (2017) 821–833. https://doi.org/10.1016/j.rser.2017.04.112.
9. H.J. Lee, D.Y. Liu, S. Yao, Flow instability of evaporative micro-channels, International Journal of Heat and Mass Transfer 53 (2010) 1740–1749. https://doi.org/10.1016/j.ijheatmasstransfer.2010.01.016.
10. B. Markal, B. Kul, M. Avci, R. Varol, Effect of gradually expanding flow passages on flow boiling of micro pin fin heat sinks, International Journal of Heat and Mass Transfer 197 (2022) 123355. https://doi.org/10.1016/j.ijheatmasstransfer.2022.123355.

11. J. Mathew, P.-S. Lee, T. Wu, C.R. Yap, Experimental study of flow boiling in a hybrid microchannel-microgap heat sink, International Journal of Heat and Mass Transfer 135 (2019) 1167–1191. https://doi.org/10.1016/j.ijheatmasstransfer.2019.02.033.
12. H.-L. Wang, H.-C. Wu, S. Kong Wang, T.-C. Hung, R.-J. Yang, A study of mini-channel thermal module design for achieving high stability and high capability in electronic cooling, Applied Thermal Engineering 51 (2013) 1144–1153. https://doi.org/10.1016/j.applthermaleng.2012.10.007.
13. S. Raj, M. Pathak, Mohd.K. Khan, Flow boiling characteristics in different configurations of stepped microchannels, Experimental Thermal and Fluid Science 119 (2020) 110217. https://doi.org/10.1016/j.expthermflusci.2020.110217.
14. M. Law, P.-S. Lee, K. Balasubramanian, Experimental investigation of flow boiling heat transfer in novel oblique-finned microchannels, International Journal of Heat and Mass Transfer 76 (2014) 419–431. https://doi.org/10.1016/j.ijheatmasstransfer.2014.04.045.
15. X.F. Peng, G.P. Peterson, Convective heat transfer and flow friction for water flow in microchannel structures, International Journal of Heat and Mass Transfer 39 (1996) 2599–2608. https://doi.org/10.1016/0017-9310(95)00327-4.
16. R.K. Shah, A.L. London, Laminar flow forced convection in ducts: a source book for compact heat exchanger analytical data, Academic Press, New York, 1978.